Turbulent, premixed, spherical NH_3/H_2 combustion; Simulation optimization and existence of 'white holes'

By R. J. M. Bastiaans and X. Liu†

1. Motivation and objectives

The subject of this research is the combustion of ammonia in combination with hydrogen as a sustainable energy carrier. Sustainable energy in the form of electricity is a great development, but combustion will undoubtedly be part of the energy mix in the future. Therefore, applications of sustainable, carbon free fuels have to be developed. The current research had the objective of improving the numerical speed and applying standard extensions when moving from application of an in-house direct numerical simulation (DNS) code in Eindhoven University of Technology to the commerical Converge computational fluid dynamics (CFD) code (Richards *et al.* 2023) for compressible turbulent combustion. This would result in a potentially dual way of dealing with the subject. On one side, the in-house DNS code uses higher order methods and is used in a quite conservative way with respect to grid resolution (including Kolmogorov and flame scales) and time stepping (including kinetic stiffness and acoustic limitations). On the other side, the commercial code is attractive from another perspective as it may be executed with a multitude of methods and approaches that can just be selected. One might find faster results without a decrease in accuracy.

Our goal was to investigate the implicitness of time steps, and the associated time step increase, resolution decrease and adaptive mesh refinement (AMR) opportunities. Furthermore, the use of flamelet generated methods (FGM), van Oijen *et al.* (2016), to reduce kinetics and large eddy simulation (LES) for resolution reduction are options to be studied later. The first of these two would be called DNS-FGM, and combined with the second one LES-FGM, when taking DNS with detailed kinetics (extended combustion DNS definition) as a reference. It is important to take the high-accuracy in-house DNS results as a reference and validate the CONVERGE results for every possible option. The approach is to evaluate and validate every consecutive substep in the order of numerics, FGM and LES. This is motivated by the decrease of potential loss of accuracy in the given order. In principle, FGM can be as accurate as needed by increasing the number of control variables. Even effects of local perturbations such as curvature and strain might be included, although in practice this is limited because the dimension of the manifold will increase to very large sizes. However, subgrid scale modeling will remain only valuable for statistical results. In the end AMR might be exchanged with filtered flamelet models, e.g., Mukhopadhay *et al.* (2015).

The considered case is that of turbulent premixed deflagration of a stoichiometric NH_3/H_2 mixture in air, shortly after ignition. The initial combustion front is taken as a perfectly spherical shape with the advantage of its property of having only one dimension, the radius, which statistically remains after subsequent turbulent development.

† Eindhoven University of Technology, The Netherlands

Therefore, averaging is easy, and many turbulent events are included in such a turbulent combustion case. Furthermore, boundary conditions become extremely simple; they are all six outflow boundaries. All in all, we consider it as a canonical case.

We also researched the way FGM should be implemented for this case and finally, we want to see how turbulence interacts with flames. In order to get a clear picture of the associated phenomena, we need to look at extended physical times.

2. Formulation and computational setup

2.1. *Reference DNS outline*

The reference case is taken from Mukundakumar & Bastiaans (2022). It was simulated with a compact implicit higher order spatial discretization method, including an explicit third-order Runge-Kutta scheme as used many times before, specifically also in the previous Center for Turbulence Research studies by Bastiaans *et al.* (2004, 2007). Again, a cubical domain was taken with Navier-Stokes characteristic boundary conditions (NSCBC) outflow boundaries everywhere (6). An equal turbulent combustion initialization was used as well, explicitly described in detail in Bastiaans *et al.* (2006), involving solenoidal velocity perturbations superimposed on a perfect spherical flame. The latter was calculated by applying the CHEM1D code (Somers 1994), with the San Diego kinetic mechanism (Jiang *et al.* 2020), for a 1D spherical flame.

The case that is specifically investigated is on turbulent premixed combustion of a kernel of a stoichiometric NH_3/H_2 mixture in air at standard ambient conditions. It is localized in the center of the cubic 15-mm^3 domain. The turbulence was windowed sufficiently smooth with a $1-tanh((r(x,y,z)-r_t)/w_t)/2-0.5$ formulation, with $r(x,y,z)$ being the radius from the origin, $r_t = 5.6$ for the transition radius and $w_t = 0.05$ for the width of the transition region. So, it is sufficiently smooth to resolve, and it contains largely the flame and burned region with a radius of $r_{il} = 1.116$ mm. This flame radius was expressed by the position of the inner layer temperature, defined as

$$T_{il} = max(\nabla T), \tag{2.1}$$

which was $T_{il} = 1091$ K. This flame structure is utilized together with the used turbulence window is displayed in Figure 1. The adiabatic laminar flame speed was calculated to be $S_l = 0.39$ m/s, with a flame thickness of $l_f = 514$ μm.

The Karlovitz number, defined as

$$Ka = \frac{l_f^2}{\eta^2}, \tag{2.2}$$

was chosen to be $Ka = 10$. In this way we were able to create a challenging flamelet regime case, because at increasing Ka above 1 it gradually enters the distributed reactions regime where flamelets cease to exist. The turbulent Reynolds number is kept low to be sure to be able to resolve turbulence: $Re_t = 4.64$. The cubical domain included a grid of 377^3, covering 14 grid points for a flame thickness and so $14/\sqrt{10} > 4$ points for the Kolmogorov scale. The time-step size was 10^{-8} s, based on earlier obtained experience that this is stable for the current grid size combined with this time discretization. Therefore the discretization was very conservative. To show the initialisation characteristics an initial resulting inner layer flame isosurface colored with the local curvature is shown in Figure 2. The initial turbulence is neither externally nor artificially internally forced and would decay if there was no kinetic energy injection from the turbulent flame

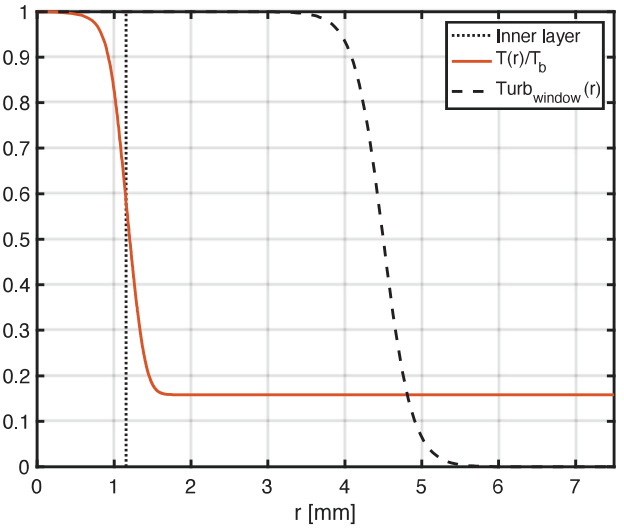

FIGURE 1. Profiles of initial temperature, nondimensionalized with $T_b = 1894$ K, and the turbulence window.

fronts. This might happen at different scales, however, originating from the occurring flame-turbulence interactions.

2.2. *Converge simulations*

The high-resolution DNS case was calculated on Advanced Micro Devices (Rome/Genua) node technology, whereas the CONVERGE simulations were carried out on AMD EPYC infrastructure. The latter simulations were all carried out on 4 nodes using 64 cores each.These were evaluated for computing time for a fair comparison.

The CONVERGE simulations were all performed with default settings for this case. These 'non-default' particular settings involved i) compressibility, ii) not using a turbulence model, iii) applying the SAGE† method for detailed chemistry, iv) inclusion of mixture-averaged transport and v) applying NSCBC boundary conditions. Additionally a default pressure-based implicit with splitting of operators (PISO) with successive over-relaxation (SOR) type of solver, as well as flux blending with a strict conserving scheme for all variables, was accepted.

We started the simulations on a base grid that is twice as coarse as our reference DNS case. This was chosen because of the conservativeness of the reference grid and to limit time requirements. The time-step size, though, was kept equal to the reference case, $\Delta t = 10^{-8}$ s. Basically the following options were tried and the required computational time for progressing over a single eddy turnover time was recorded, together with an evaluation of the result:

- Coarsening the grid size by subsequent factors of 2 (condensing storage).
- Coarsening the time step size by subsequent factors of 2.
- Fully implicit versus fully explicit time advancement schemes. Converge provides an opportunity to partial mix these two, but this was not considered as a matter of tidiness, excluding any interference.
- Applying AMR.

Furthermore an initial *a-priori* investigation for the suitability of using FGM control-

† This is no abbreviation, but a given name by the software manufacturer.

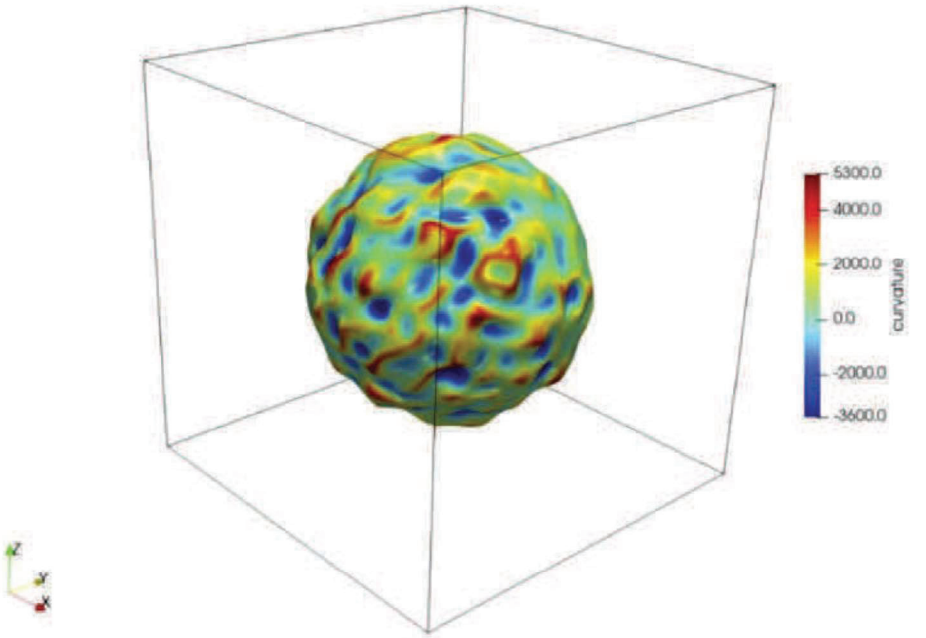

FIGURE 2. First stage of a perturbed flame shortly after perfect spherical flame initialization.

ling variables (CVs) was carried out. Simulations involving FGM with these CVs were not yet performed nor were any LES cases, including FGM. Section 3 ends with a short physical analysis of the phenomena after longer time integration.

3. Results

3.1. *Numerical*

Only qualitative observations and comparisons have been performed. Typically results were inspected at a time equal to one eddy turnover time, $t_{ETT} = 0.000283$ s, for all cases. The associated computational times are given in Table 1. This table was composed of all comparable accurate results but shows only indicative computation times, because we realized afterward that every job ID had to be stored to obtain information about the number of cores on what nodes were used. Anyway, we can see a global reduction of computing time by increasing the time-step size for the fully implicit time advancement (cases [1-4]), but not by the expected factor of 2, successively. Next we performed cases 5 and 6 for grid doublings which again showed reductions but not as expected since a factor 8 was expected subsequently. The numerics in CONVERGE seemed to switch strategy with increasing time-step sizes. In a next step, cases [7-10], we switched to fully explicit time advancements. Here quite expected computing time reductions were obtained. However, unexpectedly, the fastest accurate results were obtained by the coarsest explicit case (case 10). With these settings we advise to continue simulations, e.g., for physical investigations later in this paper. Additionally, we found no clear distinct bevavior by using AMR, as specified later.

TABLE 1. The cases considered and their results concerning computing times. *Case 6 showed first deteriorated results.

Case	Grid factor	Time step factor	Time int.	Calc. time [s]	Validation
1	1	1	implicit	121.100	V
2	1	2	implicit	45.600	V
3	1	4	implicit	55.700	V
4	1	8	implicit	39.400	V
5	2	8	implicit	23.400	V
6*	4	8	implicit	14.400	X
7	2	1	explicit	177.700	V
8	2	2	explicit	91.500	V
9	2	4	explicit	39.200	V
10	2	8	explicit	16.500	V

The initial magnitude of the velocity, from the high-resolution reference DNS is displayed in Figure 3(a). The initial two times as course initial velocity magnitudes resampled from the reference case, with which the Converge case started are given in Figure 3(b) for the three orthogonal cross sections. The first results are visualized with Matlab and the Converge results used Tecplot for CONVERGE. The used colormaps were respectively 'jet' and 'extended rainbow - dark ends', which seem to be highly equal. Note that the resampling with a factor of two does not influence the results for the initial turbulence, which is critical for $Ka > 1$, as in the current case.

The next 2-times-coarsened-associated temperature distributions obtained after one eddy turnover time can be observed in Figure 4(b) compared to the Converge reference (2 times as coarse as the high-resolution DNS) in Figure 4(a) at the left. It has to be taken in mind that in this case a grid is drawn, to visualize the grid density, that obscures a bit the flame parts near the unburnt (outer) region. The original perfect spherical flame kernel starts to deform in a 3D way induced by the initial velocity perturbations. A further factor 2 grid reduction to 4 times as coarse as the Converge reference case deteriorated the solution visibly, even if we applied AMR, locally with a factor of 2, to recover the previous acceptable global 2 times coarsening, dispayed in Figure 4(b). For the latter, a refinement was used based on exceeding a certain temperature gradient. In these cases, we doubled the grid locally in all dimensions but this was not sufficient. Likely the velocity gradients should be included as well because of their criticality when having the current Karlovitz number.

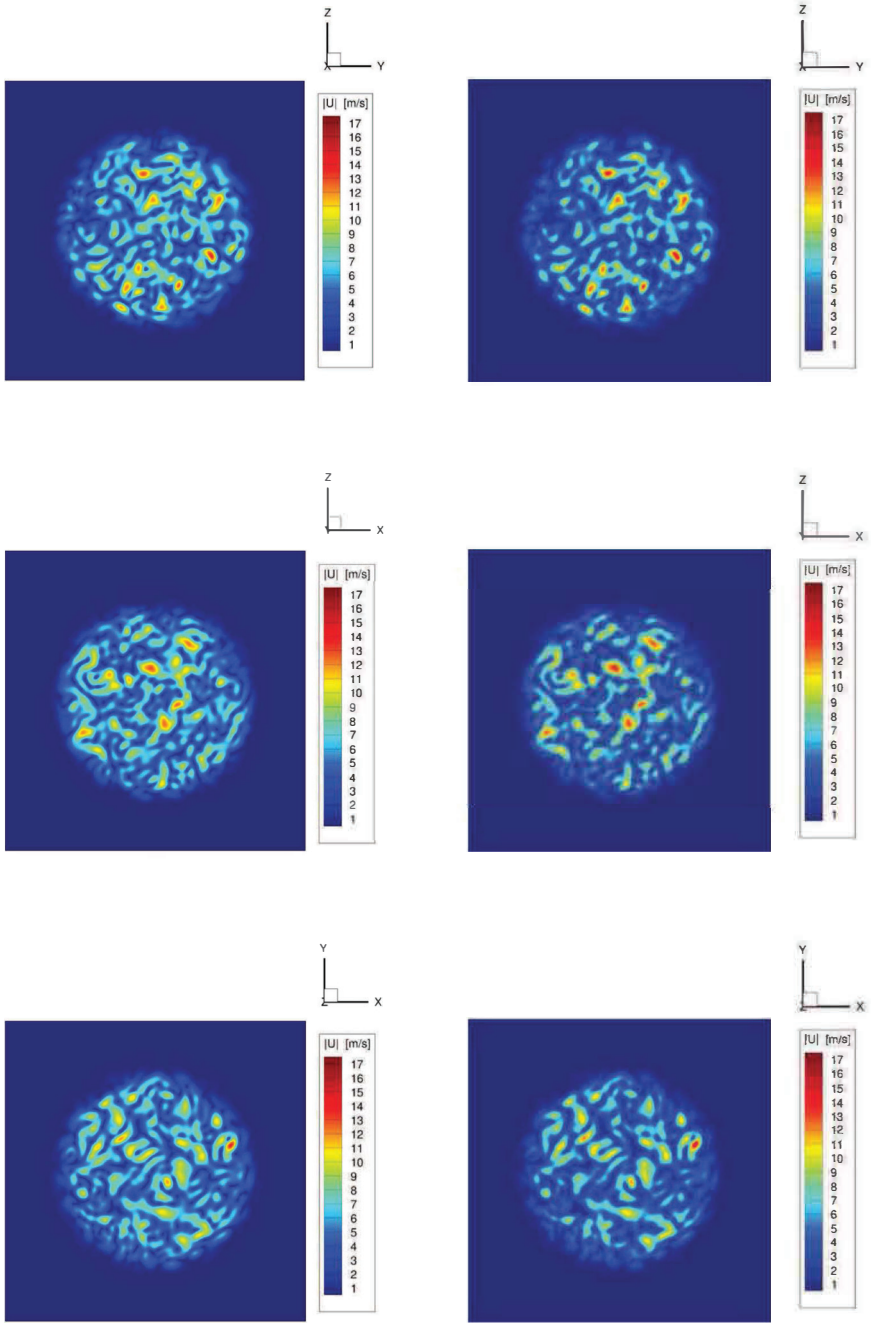

(a) (b)

FIGURE 3. Velocity magnitude cross sections along X, Y, Z midplanes (top to bottom) respectively, left: high resolution DNS, right: reference (2 times as course) Converge case.

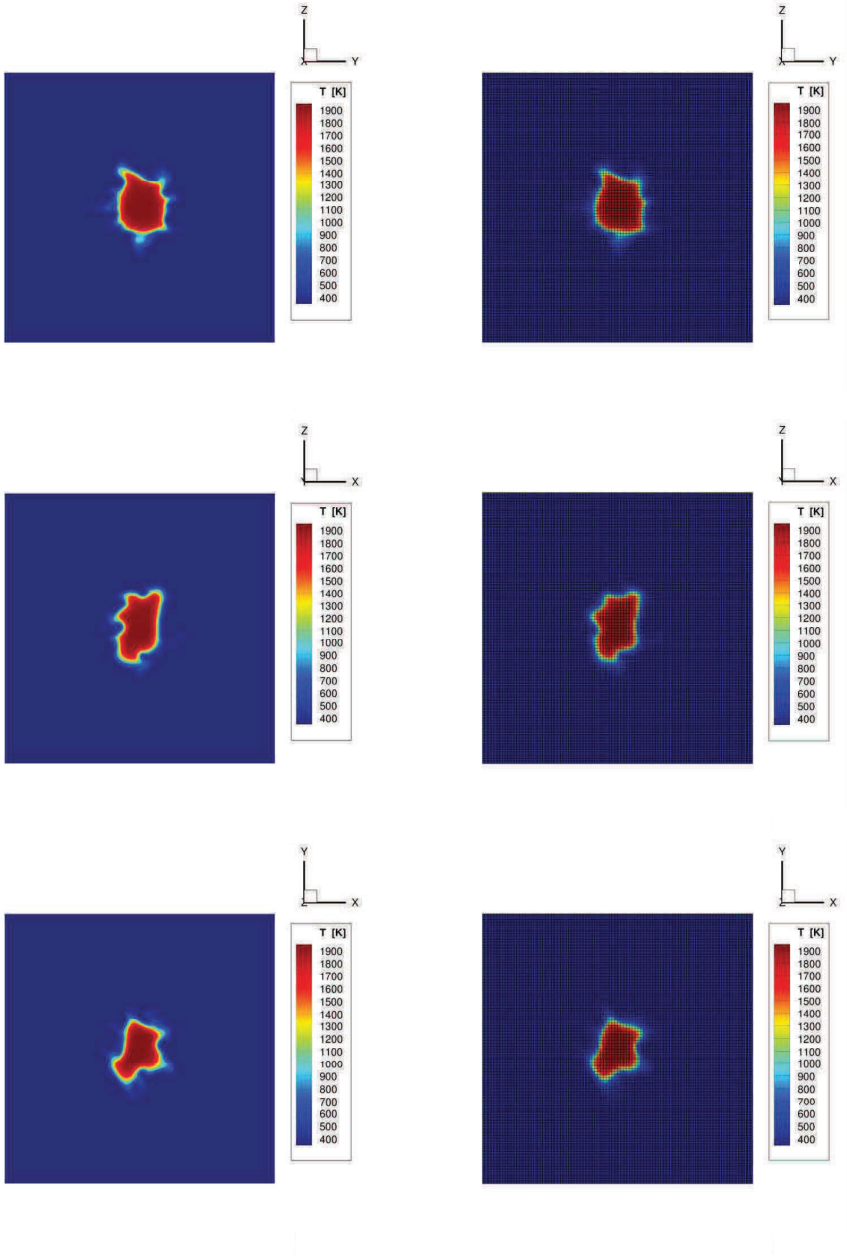

(a) (b)

FIGURE 4. Temperature field on X, Y, Z midplanes (top to bottom) respectively; (a) reference CONVERGE case, (b) the 2-times-as-coarse grid (visible grid).

Simulations involving increased time-step sizes could be attained with results visibly judged equal up to an 8 times increase as those in Figure 4. This appeared to be the case for explicit as well as implicit time steps, which of course resulted in different calculation times, as displayed in Table 1. An example of the AMR-refined grid is shown in Figure 5.

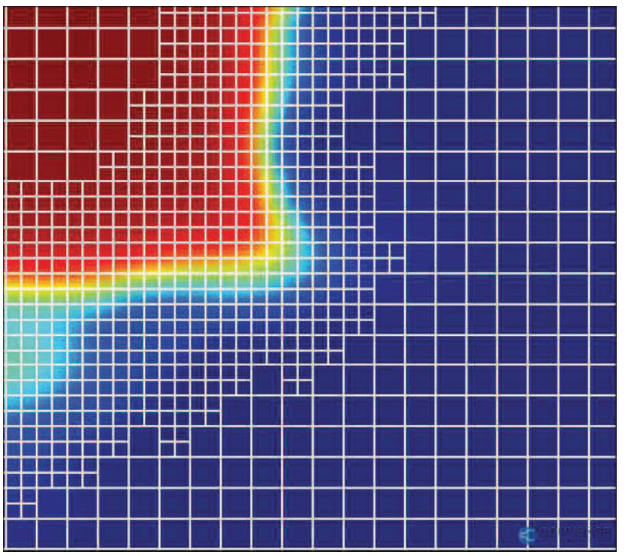

FIGURE 5. Zoomed part of X cross section of the temperature field with a visualized grid distribution refined with AMR.

3.2. *Flamelet generated manifolds*

A 'progress variable' (PV), being in general the first 'controlling variable' (CV), y, is defined as

$$y = \sum_{i=1}^{N_s} \alpha_i Y_i, \tag{3.1}$$

where α_i are the weighting coefficients of Y_i, which is the mass fraction of species i, and N_s is the total number of species. To find the optimal PV, multiple 1D manifolds based on a 1D freely premixed propagation of a NH_3/H_2 flame are first generated. Different PV formulations are compared with detailed chemistry results as an *'a-priori'* test. Our implicit understanding leads to the proposition that H_2O is a very good candidate since combustion of both fuels yield this product abundantly with only minor products like NO. The results of different possibilities are shown in Table 2 for the important quantities flame speed and flame temperature. In Table 2, "All" means a contribution of both fuels, H_2 and NH_3, the oxidizer O_2, as well as the product H_2O, weighted by their inverted molar masses. All PVs showed relatively good overall behavior, but only using H_2O predicts the studied flame properties the best. Results concerning the prediction of the temperature distribution are displayed in Figure 6(a) with a zoom in the burnt region in Figure 6(b). The temperature in the burnt region is very important for the NO_x production and as can be seen in Figure 6(b) taking NH_3 as the first CV would overpredict temperature and consequently, overpredict the amount of NO_x. Surprisingly we found the H_2O-based PV to be the default for using FGM in CONVERGE, but this might not be best for an arbitrary other fuel. Haphazardly, we could not get the FGM implementation running in the end.

In order to investigate consequences of the local turbulent flame perturbations for the applied manifolds, we decided to study the results involving curvature as a second CV. For this study, we took a PV entirely composed of H_2O as the first CV. First we looked at the occurrence of certain values of the curvature, κ, defined with the flame normal n

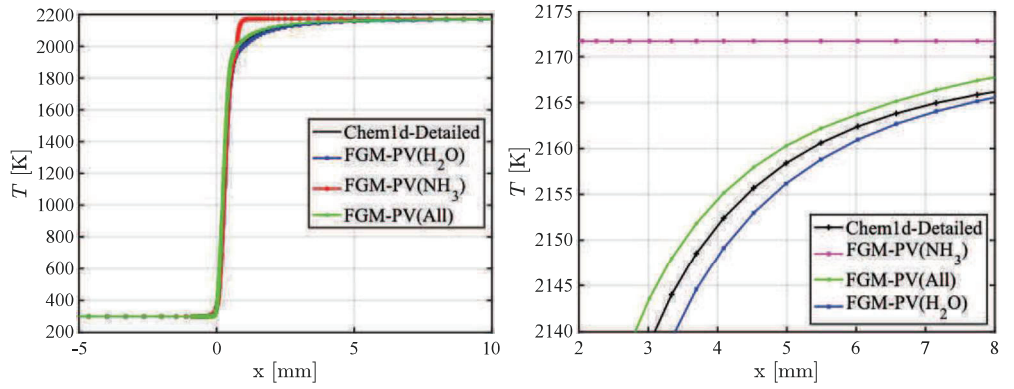

(a) (b)

FIGURE 6. Comparison for the predicted temperature distributions for different potential first FGM control variables, (a) full flame, (b) zoom of the burnt region.

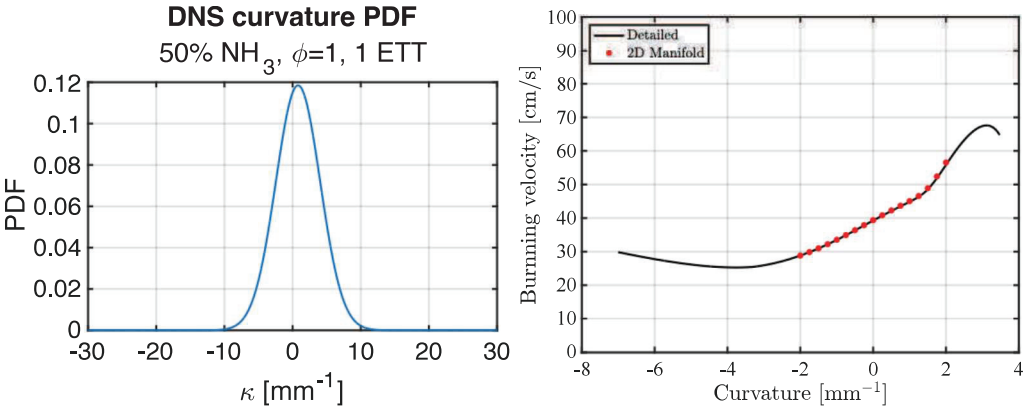

(a) (b)

FIGURE 7. (a) Observed curvature PDF for the reference high-resolution DNS case, (b) comparison of a potential additional curvature FGM control variable.

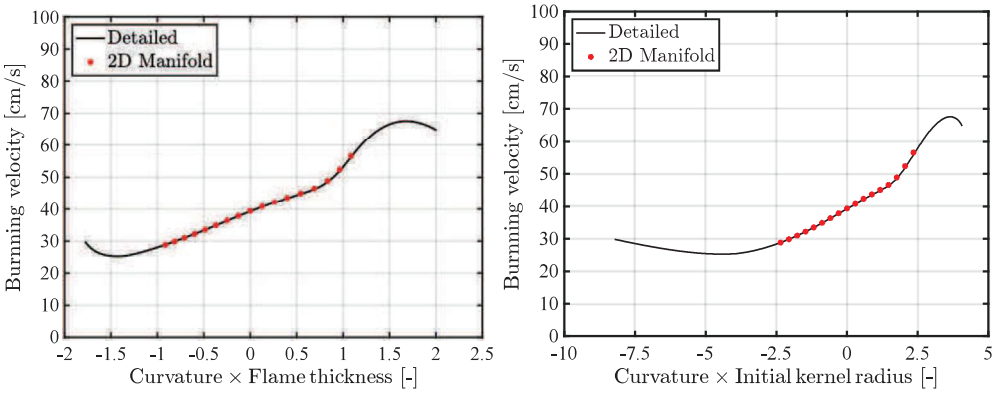

(a) (b)

FIGURE 8. Comparison of a potential additional curvature FGM control variable, (a) scaled with flame thickness, (b) scaled with initial kernel size.

TABLE 2. Comparison of adiabatic 1D flame results between different kinetics treatments.

	Flame temperature [K]	Laminar flame speed [cm/s]
Detailed chemistry	2171.7	39.26
FGM CV H_2O	2172.1	39.37
FGM CV NH_3	2171.7	38.52
FGM CV all	2172.0	35.98

as

$$n = -\frac{\nabla y}{|\nabla y|}, \tag{3.2}$$

attributed to an increasing quantity y toward the unburned side (e.g., density), as

$$\kappa = \nabla \cdot n. \tag{3.3}$$

Its probability in the current case is shown in Figure 7(a). Clearly it is quite Gaussian distributed, with a slight preference for positive values, which can be assigned to the positive initial global flame curvature, associated with the initial radius. Then we considered inclusion of this curvature variable, κ in the manifold by filling it as a second dimension. This could be included as a standard feature in CHEM1D. The resulting graph, for the prediction of the burning velocity, is shown in Figure 7(b), first not scaled at all, so it is easy to compare to Figure 7(a). Note that the curvatures easily and accurately form a compact required value range around the maximum curvature values that were obtained in the detailed chemistry DNS. We have to extend this to a larger range, though.

Next a nondimensionalized plot with the (initial) flame thickness in Figure 8(a). This is already quite curved, having a high curvature typically ranging from [−1,1] flame thickness. For the detailed simulation, this could be executed without a problem, but for curved 1D flames (in CHEM1D) this easily runs into trouble at higher values, but even values somewhat extending 1 could be attained. A scaling with the initial kernel radius used is displayed in Figure 8(b). The results showed a favorable approach. This therefore seems to be a very promising method for involving a 2D FGM in the simulation of our turbulent combustion case. We can easily implement it in the in-house high-resolution code, but not yet in CONVERGE.

3.3. *Physical*

To investigate the behavior of the flame kernel and the turbulence in the longer term, we took long integration times however, we had to stop when a single extreme radial event hit the boundary, which occurred shortly after six eddy turnover times. In Figure 9(a,b), the temperature fields and velocity magnitudes are provided, respectively. In the temperature fields, the turbulent propagation extension of the burned region is visible. The velocity magnitude shows decayed values of course. The turbulence extension is, however, also clearly visible, which was less expected. Moreover, as a result relevant turbulence intensities are only left at the unburned zone.

Implications for the flame kinetic energy backscatter in nonreacting and so cold flow can be derived by looking at the cold flow velocity magnitude fluctuations, shown in Figure 10, as compared to this previous reacting case. As a characteristic result, only results for the middle Z plane are shown. In the cold case, the decay of large values is

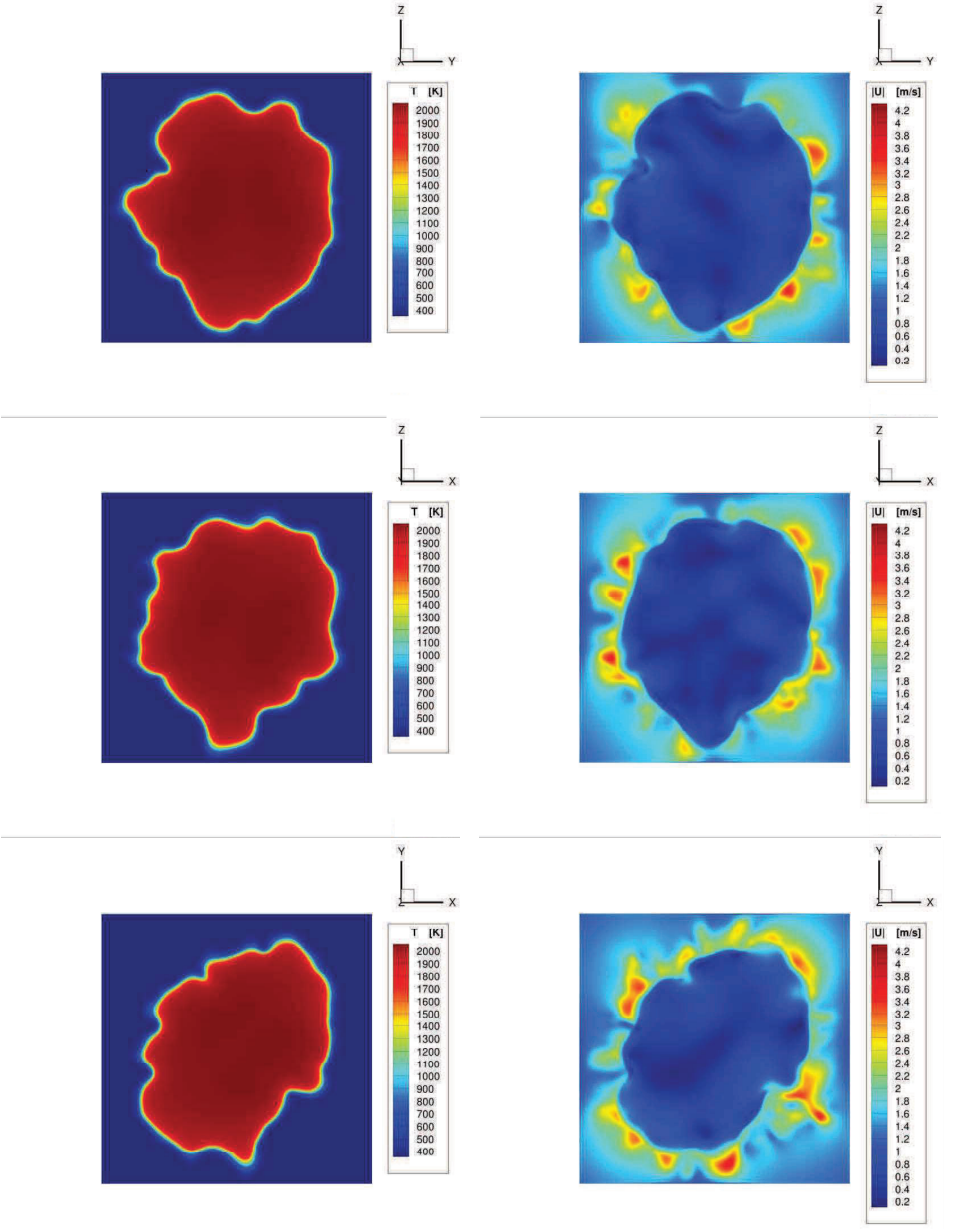

FIGURE 9. Distributions of variables in the selected planes at t equal to six eddy turnover times; (a) temperature, (b) velocity magnitude.

clearly larger, mitigated from 4.2 to 2 m/s, originating at $t = 0$ from about 17 m/s. Also it stays quite compact in the initial region. For the reacting case fluctuating velocity magnitudes in the burned region do not reach a value of 2 m/s and the structure of the turbulence (length scales) is clearly less pronounced. For this case, it might/should be checked whether the NSCBC boundary conditions had an influence on the observed outer

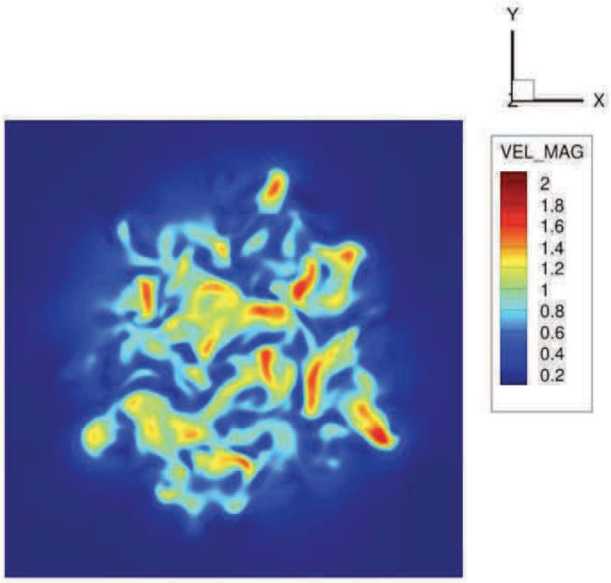

FIGURE 10. Distribution of the velocity magnitude in the middle Z plane at t equal to six eddy turnover times for the nonreacting case.

region turbulence by extending the domain size. Clearly flame turbulence interaction is manifest. A sensible thing to do it more formally is by filtering a 3D field, evaluating the velocity magnitude, considered here, in 3D and applying statistics to condense everything to 1D as a function of the radius.

Altogether, the observed building blocks lead to a phenomenon that might be associated with turbulent premixed flame kernels could be thought of as acting as 'white holes' as opposed to 'black holes'. This in the sense that 'white holes' emit (turbulence) information to their outskirts and prevent the reentry of this information. Its observation horizon could probably be associated with the flame inner layer. More research is required to better substantiate this suggestion, which is why we only provide it as a conjecture.The concept of entropy transport, including production and consumption, and its behavior within the flame kernel inner layer as well as globally is advised to be investigated for this phenomenon. Whatever is found by these investigations, the separate factors of Re and Ka numbers should constitute a combined quantity because of their observed severe mutual interaction.

4. Discussion

Clearly the initial high-resolution DNS with higher order approximations was very conservative for its grid size. Optimization in calculation speed and comparing different numerical codes for it involves a threefold evaluation. First there is the verification step, in which it should be checked whether the intended equations are solved, at least when sufficient resolution is applied. The second step concerns validation, which might be performed by comparing solutions of different codes, and would preferably be done with experiments, which can only be performed for applied cases and less or none for canonical cases. The third one is optimization of implementations, e.g., with respect to CPU cache use, GPU use and maybe quantum computer technology and AI.

Furthermore, AMR should be carefully applied to selecting the right variables with correct refinement criteria to obtain the desired speed up. For the latter, the homogeneity of the gradients of the selected variables should also be taken into account as well as the isotopy of these variable, e.g., for cold homogeneous turbulence, a global equidistant grid cannot be optimized very much with AMR. For unidirectional flame variable gradients in case of combustion fronts, pay attention to the value of the Karlovitz number in combination with the occupation of the front in the computational domain. This interferes with phenomena associated with the mentioned isotropy issue for flame variable gradients, which might be unidirectional. In combination with the local grid orientation, this might require potentially limited refinement directions.

Finally, we have to consider LES SGS models. But this can only be compared in a statistical way, making it less trustworthy, although subgrid contributions might be compared to modeled values using a statistical approach. SGS controlling variables probability density functions (PDFs) and SGS flame turbulence interactions (FTIs) have to be taken into account as well.

Ultimately for the prediction of NO_x emissions, providing a design tool for optimizing the selection of design and operational parameters is of course the challenge for this carbon-free fuel, including fuel nitrogen. For this case, the FGM predictions for these emissions is very important as well. A potential solution would be to take a transport term for these species into account in simulations and include their source terms in the manifold as used initially by Vreman *et al.* (2007) and later by, e.g., Donini *et al.* (2017).

5. Conclusions

The initial high-resolution DNS was very conservative at least for its grid size and maybe a bit conservative for its time-step size, the latter considering the Courant-Friedrichs-Lewy (CFL) condition for the high resolution. Additionally, for this limited study some calculating speed up methods are identified. Time-steps can be increased by a factor of 8 with a doubled grid size (4 times relative to our high-resolution DNS case), leading to a speed up that can not yet be explained, though explicit time discretization seems to be optimal. But this conclusion has to mitigated, because the reference case is quite over-resolved and the timing results could not be compared exactly. Concerning speed up with FGM, we can conclude that 1D *a-priori* testing of a 2D manifold containing H_2O and flame curvature as controlling variables would be an accurate set and would providie great potential for application in DNS-FGM. This should be tested *a posteriori* in an actual DNS-FGM simulation; it can be tested and compared at a realization level.

Finally, there remains the physical issue of the (corrugated) flame backscatter of SGS turbulent kinetic energy to the resolved scales. All data is available, though the exact analysis including convoluting of the DNS has yet to be executed. Although from the comparison of the velocity magnitudes, there is clearly a considerable flame turbulence interaction. This might have important implications for LES SGS models.

Observations of the behavior of unforced, or natural, turbulence lead to us raising the concept of 'white holes' associated to turbulent premixed flame kernels. The term was coined apart from specific semantics and/or connotations. Probably it promotes a return to a state of perfect spherical propagation. In any case, the concept of the Borghi diagram and its implied regional behavior, with independency of Re and Ka, should be reconsidered.

REFERENCES

Bastiaans, R.J.M., Somers, L.M.T. & de Lange, H.C. 2001 DNS of non-premixed combustion in a compressible mixing layer. In *Mod. Simul. Strat. Turbul. Flow* (ed. B.J. Geurts), pp. 247–261. Philadelpha, PA: R. T. Edwards Publishers.

Bastiaans, R.J.M., van Oijen, J.A., Martin, S.M., de Goey, L.P.H. & Pitsch, H. 2004 DNS of lean premixed turbulent spherical flames with a flamelet generated manifold. *Annual Research Briefs*, Center for Turbulence Research, Stanford University, pp. 257–268.

Bastiaans, R.J.M., van Oijen, J.A. & de Goey, L.P.H. 2006 DNS simulations of lean premixed flame kernels with flamelet generated manifolds; an overview. *Proceedings European Conference on Computational Fluid Dynamics (ECCOMAS CFD 2006, Egmond aan Zee, The Netherlands, September 5-8).* Wesseling, P., Oñate, E. & Périaux, J. (eds.). Delft: Technische Universiteit Delft, pp. 1–22.

Bastiaans, R.J.M., Vreman, A.W. & Pitsch, H. 2007 DNS of lean hydrogen combustion with flamelet-generated manifolds. *Annual Research Briefs*, Center for Turbulence Research, Stanford University, pp. 195–206.

Donini, A., Bastiaans, R.J.M., van Oijen, J.A. & de Goey, L.P.H. 2017 A 5-D implementation of FGM for the large eddy simulation of a stratified swirled flame with heat loss in a gas turbine combustor. *Flow Turbul. Combust.* **98**, 887–922

Jiang, Y., Gruber, A., Seshadri, K. & Williams, F. 2020 An updated short chemical-kinetic nitrogen mechanism for carbon-free combustion applications. *Int. J. Energ. Res.* **44**, 795–810

Mukhopadhyay, S., Bastiaans, R.J.M., van Oijen, J.A. & de Goey, L.P.H. 2015 Analysis of a filtered flamelet approach for coarse DNS of premixed turbulent combustion *Fuel* **144**, 388–399

Mukundakumar, N. & Bastiaans, R.J.M. 2022 DNS study of spherically expanding premixed turbulent ammonia-hydrogen flame kernels: Effect of equivalence ratio and hydrogen content. *Energies* **15** (13), 4749.

Richards, K.J., Senecal, P.K., Pomraning, E. 2023 CONVERGE (Version 3.1) Manual. Convergent Science Inc.

Somers, L.M.T. 1994 *The Simulation of flat Flames with Detailed and Reduced Chemical models.* Ph.D. Thesis, Eindhoven Univ. Technol., Eindhoven, The Netherlands.

van Oijen, J.A., Donini, A., Bastiaans, R.J.M., ten Thije Boonkkamp, J.H.M. & de Goey, L.P.H. 2016 State-of-the-art in premixed combustion modeling using flamelet generated manifolds. *Prog. Energ. Combust.* **57**, 30–74.

Vreman, A.W., Albrecht, B.A., van Oijen J.A., de Goey L.P.H. & Bastiaans, R.J.M. 2008 Premixed and nonpremixed generated manifolds in large-eddy simulation of Sandia flame D and F. *Combust. Flame* **153**, 394–416.